# The Three-dimensional Structure of the Nemaline Rod Z-Band

**E. P. Morris, G. Nneji, and J. M. Squire**

Biophysics Section, The Blackett Laboratory, Imperial College, London SW7 2BZ, England

***Abstract.*** In nemaline myopathy and some cardiac muscles, the Z-band becomes greatly enlarged and contains multiple layers of a zigzag structure similar to that seen in normal muscle. Because of the additional periodicity in the direction of the filament axis, these structures are particularly favorable for three-dimensional analysis since it becomes possible to average the data in all three dimensions and thus improve the reliability of the reconstruction. Individual views of the structure corresponding to tilted longitudinal and transverse sections were combined by matching the phases of common reflections. Examination of the tilted views strongly suggested that to the available resolution, the structure possesses fourfold screw symmetry along the actin filament axes. This symmetry could be used both in establishing the correct alignment for the combination of individual tilted views and to generate additional views not readily accessible in a single tilt series. The reconstruction shows actin filaments from one sarcomere surrounded by an array of four actin filaments with opposite polarity from the adjacent sarcomere. The actin filaments show a right-handed twist and are connected by a structure that links adjacent filaments with the same polarity at the same axial level, then runs parallel to the filaments, and finally forms a link between two actin filaments whose polarity is opposite to that of the first pair. The connecting structure is probably composed of $\alpha$-actinin which is located in Z-bands and cross-links actin filaments. The connecting structure may consist of two $\alpha$-actinin molecules linking actin filaments of opposite polarity.

NEMALINE myopathy, a congenital muscle disease, is characterized by an enlargement of the muscle Z-band. Similar enlarged Z-bands are also seen in other muscle diseases and in cardiac papillary muscle. These enlarged Z-bands often extend to several microns in the direction of the muscle fiber long axis, compared with the normal Z-bands widths in the range between 40 and 120 nm. In various previous studies of their appearance, it has been concluded that the nemaline Z-bands are closely related in structure to the normal Z-band, the extended size arising from the addition of multiple layers of the normal Z-band repeating unit (Goldstein et al., 1980; Squire, 1981).

Goldstein et al. (1980) have analyzed the appearance of nemaline rods extracted at low ionic strength in longitudinal section and concluded that the structure is composed of filaments arranged in a centered square lattice with lateral dimension of 24 nm. They also observed an axial repeat of 38 nm corresponding to a zigzag motif similar to that seen in other Z-bands. They compared the nemaline rod structure to the Z-band in rat and rabbit soleus muscle. Yamaguchi et al. (1978) have treated glycerinated nemaline rods with calcium-activated factor (CAF), a $Ca^{2+}$-activated neutral protease, which releases $\alpha$-actinin from the Z-band. Before treatment with CAF the nemaline rods showed an axial periodicity of 34.5 nm (presumably the same repeat observed by Goldstein et al., 1980). Treatment with CAF removed this axial periodicity, while leaving longitudinal filaments. Decoration with heavy meromyosin was used to demonstrate that these filaments were composed of actin.

These structures appear to be naturally occurring crystals, composed of multiple layers of the Z-band structure. They are particularly favorable for three-dimensional analysis compared with normal Z-bands, since it is possible to average data in all three dimensions. We have carried out three-dimensional reconstructions from thin sections through the nemaline Z-band: the resulting stain density map shows new details of the arrangement of actin filaments and of the structures which link them. From the studies of Yamaguchi et al. (1978), it can be inferred that the linking structures are partly or wholly composed of $\alpha$-actinin: thus from the shape of the linking structures we are able to identify new details of the interaction between $\alpha$-actinin and the actin filament.

## *Materials and Methods*

### *Electron Microscopy*

Blocks of araldite embedded biopsy specimens from patients with nemaline myopathy were obtained from Dr. M. Cullen (Newcastle General Hospital, Newcastle). Sections of ~80 nm in thickness cut in both transverse and longitudinal directions were used for the analysis. Electron micrographs were obtained using a JEOL 1200EX microscope with a goniometer and a rotating specimen holder. In order to facilitate collection of tilt series about a defined axis with respect to the specimens, we fitted a cross-hair graticule to the binocular system, which we then aligned with the goniometer tilt axis by observing the direction of motion of particles when the stage translation

controls were adjusted. We could then align periodic features in the Z-bands with the cross-hair. Tilt series were recorded in the range ± 60° with increments of 5° using Agfa electron microscope film at a nominal magnification of 30,000. The unit cell dimensions in the Z-crystal were determined with reference to the 14.5-nm periodicity of the myosin heads in the A-band, which in some cases was recorded in the same field as the longitudinal sections of the Z-crystal.

### *Image Analysis*

Images were analyzed using VAX 11/750 and Microvax 2000 computers. Electron micrographs were digitized on a rotating drum densitometer (Joyce-Loebl Scandig 3, Gateshead, UK) with a spot size and scanning increment of 25 μm. Image display and manipulation were carried out with a graphics terminal (Sigma 5668) or a Vaxstation 2000 workstation. Programs from the Medical Research Council Laboratory of Molecular Biology (Cambridge, UK) were used for masking and floating data, fast Fourier transforms, extraction of reflections from Fourier transforms and 3-dimensional synthesis as described in Amos et al. (1982). Locally developed programs were used for image display and combining Fourier transform data from tilted views using common reflections. Three-dimensional reconstructions were displayed and examined using Frodo on an Evans and Sutherland PS300 graphics system.

## *Results*

The overall appearance of the nemaline rods in longitudinal section is illustrated in the low magnification electron micrograph in Fig. 1. The myofibrils towards the top right hand corner show relatively slight widening of the Z-band. Much greater widening, up to about one-third of a sarcomere, is seen in the myofibrils to the centre of the micrograph.

### *Transverse Views*

Analysis of transverse sections of electron micrographs of the Z-crystals (Fig. 2 *A*) reveals a structure similar to the small-square lattice previously described by various authors (Landon, 1970; Ullrick et al., 1977; Goldstein et al., 1979) for transverse sections of the Z-band. The computed diffraction patterns (Fig. 2 *b*) of such images show strong [2,0], [0,2], [1,1] and [-1,1] reflections, while other reflections are weak or absent: this type of pattern appears to be characteristic of the small-square lattice. Goldstein et al. (1979) noted similar features in their optical diffraction patterns of the small square lattice from cardiac Z-bands. The computed diffraction pattern shows that the lattice in the electron micrograph is not truly square: the $a^*$ and $b^*$ axes are not equal and the cell angle is not exactly 90°. This effect was commonly seen and probably arises from compression in the section. Fourier-filtered images were calculated from the computed diffraction pattern as described by Misell (1978). In these images (Fig. 2, *c* and *d*) the distortion in the lattice has been corrected. Fig. 2 *c* is the Fourier-filtered image derived directly from Fig. 2 *a*, whereas in Fig. 2 *d* these data have been combined with data from the longitudinal tilt series (see below). In Fig. 2, *c* and *d*, actin filaments (seen as dark against a light background) enter from one side of the Z-band and occupy the central position in the square lattice (marked with a box), whereas filaments from the other side are located at the corners of the square. Prominent links appear to run between like filaments with a noticeable increase in protein density where the strands appear to cross each other. This appearance is very similar to processed transverse images of the small square lattice in rat soleus muscle (Goldstein et al., 1987).

### *Longitudinal Views*

In longitudinal section of the nemaline Z-crystals, several different appearances were seen. These appearances could be understood by analyzing a series of images tilted about an axis parallel to the filaments and comparing their com-

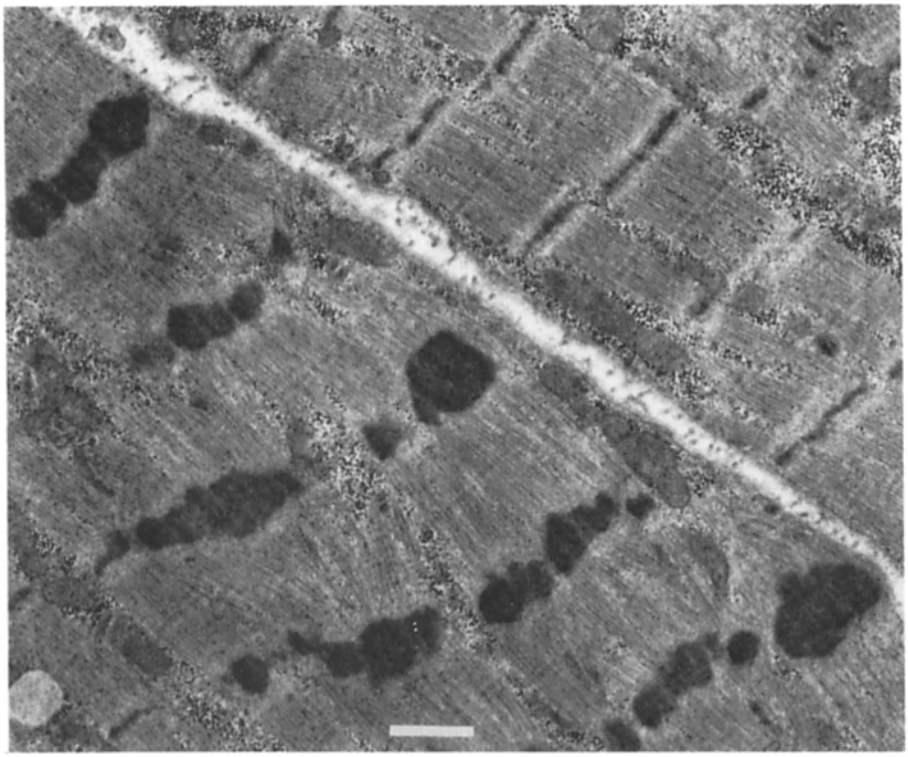

*Figure 1.* Nemaline myopathy. Low-magnification micrograph of a longitudinal section showing regions of enlarged Z-bands together with a region of more normal appearance (*top right*). Bar, 1,000 nm.

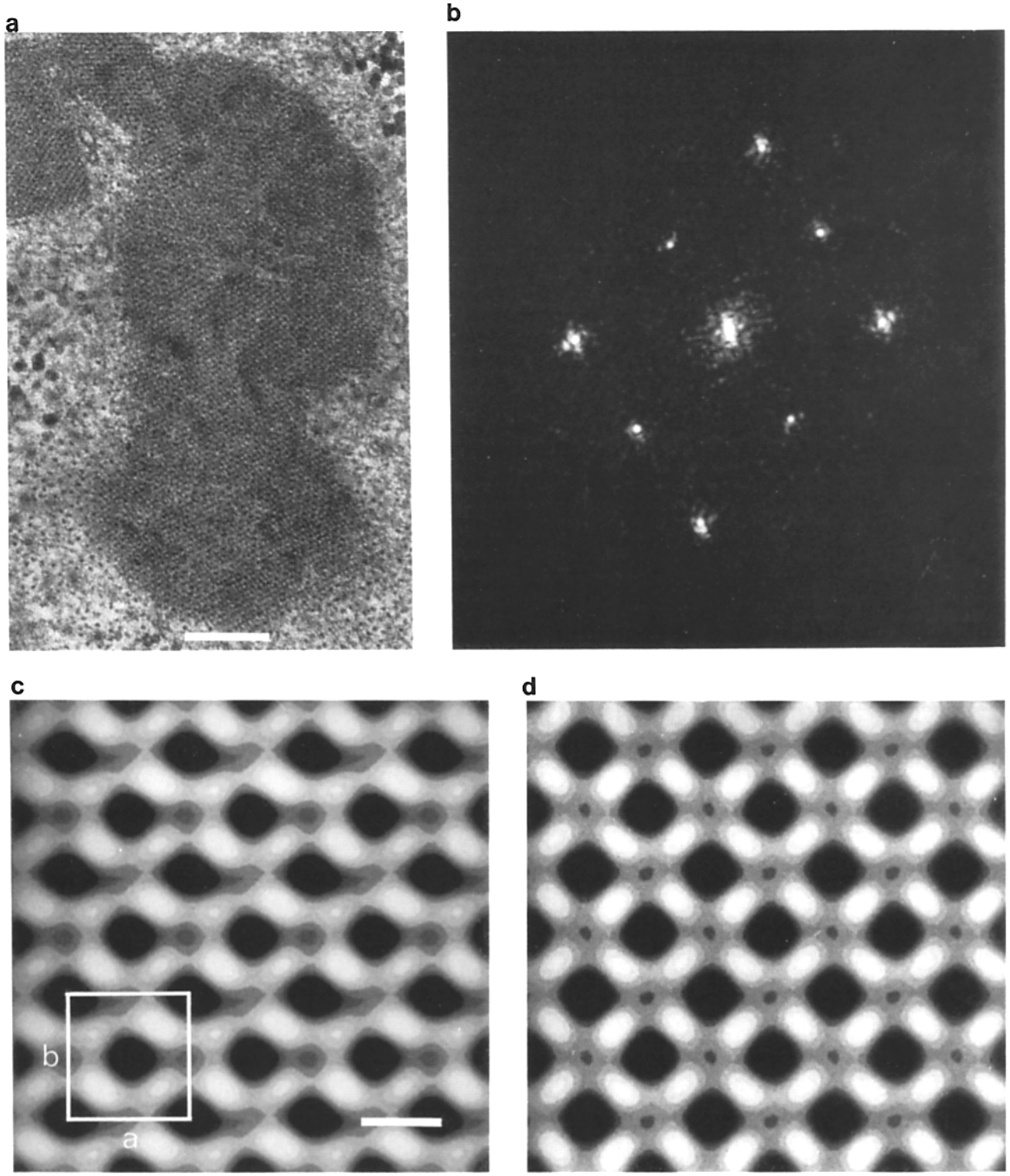


*Figure 2.* Transverse view of the nemaline Z-band. (*a*) Micrograph of transverse section; (*b*) computed diffraction pattern of *a*; (*c*) Fourier-filtered image of *a* in which the effects of lattice distortion (unequal $a^*$ and $b^*$ axes and departure from 90° of the lattice angle) have been corrected. (*d*) Two-dimensional Fourier synthesis from data in *a*, combined with data from a tilt series of a longitudinal section. Dark areas represent protein density. In *c* and *d*, actin filaments are viewed end on in a centered square lattice, which is identified in *c* with a box marking a unit cell. Two sides of the box corresponding to the *a* and *b* axes are labeled. The actin filaments are approximately square in profile with the sides of the squares running parallel to the diagonals of the unit cell. Linking material is located in the central position between filaments and appears to make contacts with each of the surrounding four filaments. Bars: (*a*) 200 nm; (*c* and *d*) 20 nm.

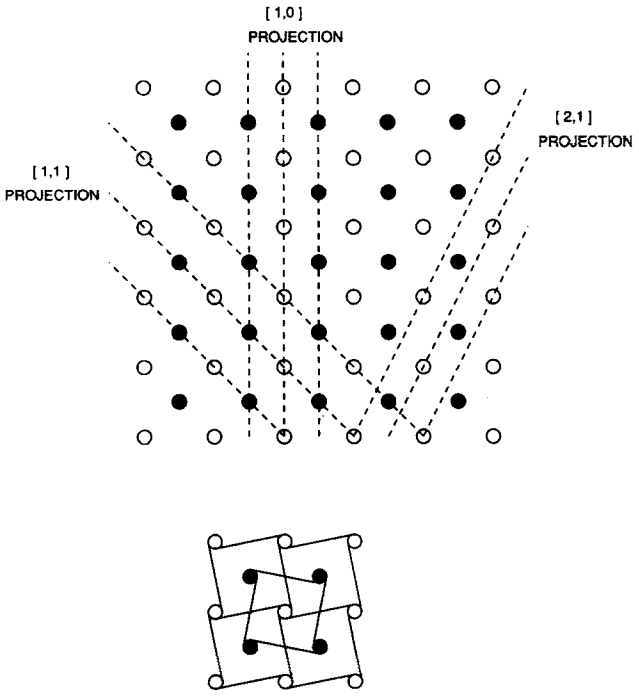


*Figure 3.* Diagrams of the transverse view of the nemaline Z-band structure: actin filaments are viewed end on. Actin filaments deriving from one side of the Z-band (*open circles*); actin filaments from the other side (*closed circles*). In *a* the dashed lines show the different directions of projection observed in longitudinal sections and used in the three-dimensional reconstructions. In *b*, solid lines show the apparent linking pattern between filaments.

puted diffraction patterns and filtered images with those of the transverse sections. Three characteristic appearances were identified and assigned to particular projections through the transverse structure illustrated in Fig. 3, which also shows the pattern of connection of the linking structures in this view. The first (Fig. 4 *a*, in this case an untilted view) was identified as a [1,0] or [0,1] type projection of the structure. Its computed diffraction pattern (Fig. 4 *b*) shows a strong second order reflection on the equator but a weak or absent first order: also on the meridian the second order reflection is strong, whereas the first order is weak or absent. The appearance of the meridian is the same in the computed diffraction patterns of the other members of this tilt series: this arises because the meridian coincides with the tilt axis and so the same region of reciprocal space is being sampled. In the Fourier-filtered image (Fig. 4 *c*) the unit cell contains two filament projections: these are of opposite polarity and derive from adjacent sarcomeres. Adjacent filaments are spaced 14 nm apart and the unit cell is 28 nm wide. Links between filaments at 39 nm intervals connect with filaments that alternate in appearance, having increased density either directly above or below the link: this gives rise to the appearance of zigzags that run across the crystal. The filaments also show a second region of increased density halfway between the zigzag motifs. In this type of view it is possible to determine which filament projection in the Z-band derives from which sarcomere by examination of the edges of the Z-band (Fig. 4 *a*) where alternate filament projections can be identified as being continuous with filaments emerging at each end. Relating these features to the filtered images shows that the zigzag motifs associated with each filament "point" to the end of the Z-band where they are associated with an emerging actin filament. In this respect the zigzag motif is similar to the type of zigzag seen in normal Z-bands.

The second type of longitudinal view (Fig. 5 *a*, which corresponds to Fig. 4 *a* tilted to 50°) was identified as a [1,1] type projection. In this case the first equatorial reflection in the computed diffraction pattern (Fig. 5 *b*) is strong and the unit cell in the Fourier-filtered image (Fig. 5 *c*) contains a single filament profile that derives from the superposition of filaments originating from each side of the Z-band. The filaments are spaced 20 nm apart. The filaments appear to lack continuity, showing regions of enhanced density extending ~30 nm alternating with regions of reduced density extending ~9 nm. However, since it is shown later that filaments in the three-dimensional reconstruction are continuous, it would seem that the apparent lack of continuity in this view arises because much of the stain density derives from the linking material rather than the filaments.

The third type of longitudinal view (Fig. 6 *a*, which corresponds to Fig. 4 *a* tilted to 40°) was identified as a [2,1] type projection. In the Fourier-filtered image (Fig. 6 *c*) projections of filaments are spaced 12.5 nm apart and appear as inverted Y shapes with linked arms. The [1,2]-type projection obtained in the same tilt series was very similar in appearance except that the polarity of the Y motif was reversed. As in the case of the [1,1] type view, it is difficult to identify continuous filament profiles: here the filaments are even more closely spaced so that again most of the contrast derives from the linking structures.

### *Relating the [1,0] and [0,1] Longitudinal Views*

A second tilt series of a longitudinal section again tilted about an axis parallel to the filament axes was used to relate the [1,0] and [0,1] views. In this case the untilted view was identified as the [1,1]-type projection and the [1,0] (Fig. 7 *a*) and [0,1] (Fig. 7 *b*) views corresponded to −50° and +55° tilts, respectively. These two views, their computed diffraction patterns (Fig. 7, *c* and *d*) and Fourier-filtered images (Fig. 7, *e* and *f*) are very similar to each other and also to other [1,0] type views that we obtained (e.g., Fig. 4). These observations can be explained by the structure possessing either fourfold rotation or fourfold screw symmetry. In the computed diffraction patterns of the longitudinal views (Figs. 4 *b*, 5 *b*, 6 *b*, and 7, *c* and *d*) the second order reflection on the meridian is always strong, whereas the first order is weak or absent. Absence of this reflection is consistent with but does not prove fourfold screw symmetry. Two methods were used to establish the symmetry of the structure.

In the first method, the [1,0] and [0,1] views in the tilt series were aligned with each other by aligning common features (e.g., glycogen or stain granules) in successive members of the tilt series. What was judged to be the same region in each of these views was then masked off and the diffraction patterns and filtered images of these regions were calculated. These are shown in Fig. 7, *c–f*. Examination of the filtered images shows that the zigzag motif in the [1,0] view (Fig. 7 *e*) is translated by half a unit cell in the [0,1] view (Fig. 7 *f*). In addition, tilting between the [1,0] and [0,1] views converts the zigzag motif into the regions of increased density be-

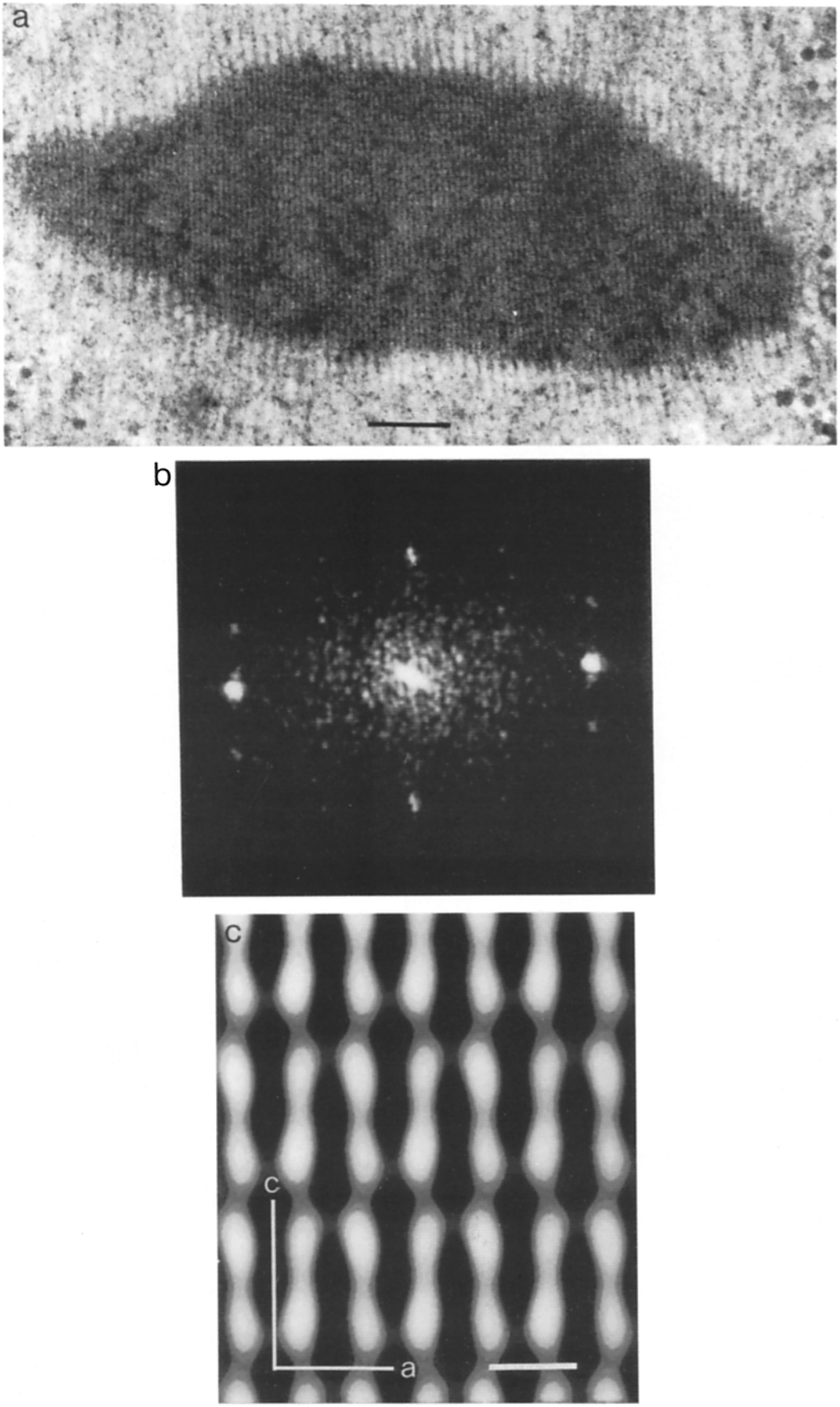


*Figure 4.* Longitudinal [1, 0]-type view of the nemaline Z-band. (*a*) Micrograph of a longitudinal section. Filaments can be seen running through the enlarged Z-band and these are continuous with actin filaments emerging from one or other side. (*b*) Computed diffraction pattern of *a*. (*c*) Fourier-filtered image of *a*. Dark areas represent protein. The *a* and *c* axes of the three-dimensional unit cell are marked. Adjacent filaments running vertically have opposite orientations and links between filaments together with increased density above and below the links to alternate filaments contribute to the zigzag patterns running across the structure and spaced at 39-nm intervals along the filaments. Bars: (*a*) 200 nm; (*b*) 20 nm.

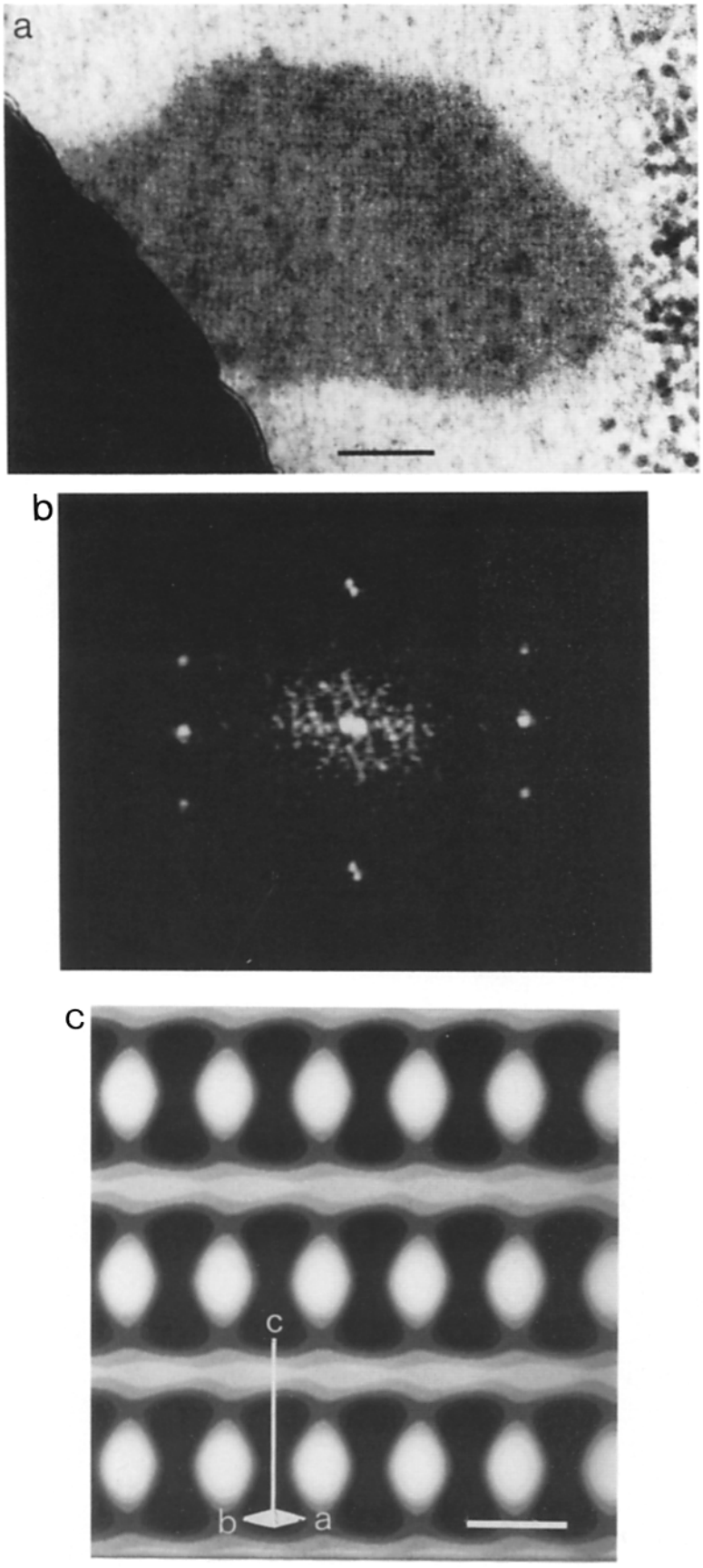


*Figure 5.* Longitudinal [1,1]-type view of the nemaline Z-band. (*a*) Micrograph corresponding to the section in Fig. 4 tilted through 50° about a filament axis. Filaments run through the Z-band and a pronounced cross-striation can be seen. (*b*) Computed diffraction pattern of *a*. (*c*) Fourier-filtered image of *a*. Dark areas represent protein. The *a*, *b*, and *c* axes of the three-dimensional unit cell are marked. The tilt axis of the micrograph is parallel to the *c* axis. Adjacent filaments running vertically correspond to projections of superposed filaments that have opposite polarity. Adjacent projections of filaments are equivalent and show no polarity. Links between adjacent filaments occur above and below regions of reduced filament density. Bar, 20 nm.

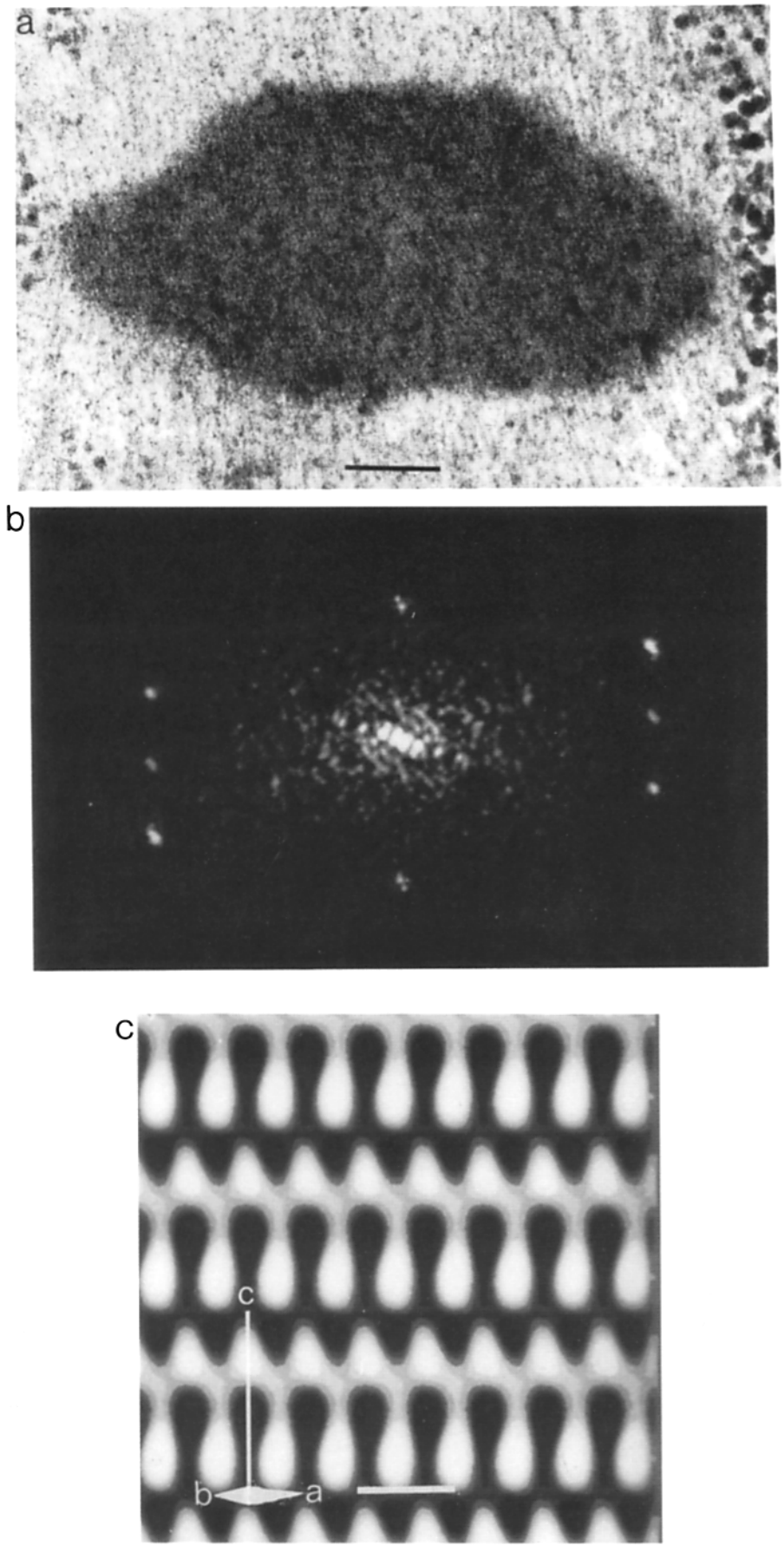


*Figure 6.* Longitudinal [2,1]-type view of the nemaline Z-band. (*a*) Micrograph corresponding to the section in Fig. 4 tilted to 25° about a filament axis. (*b*) Computed diffraction pattern of *a*. (*c*) Fourier-filtered image of *a*. Dark areas represent protein. The *a*, *b*, and *c* axes of the three-dimensional unit cell are marked. The tilt axis in the micrograph is parallel to the *c* axis. Bar, 20 nm.

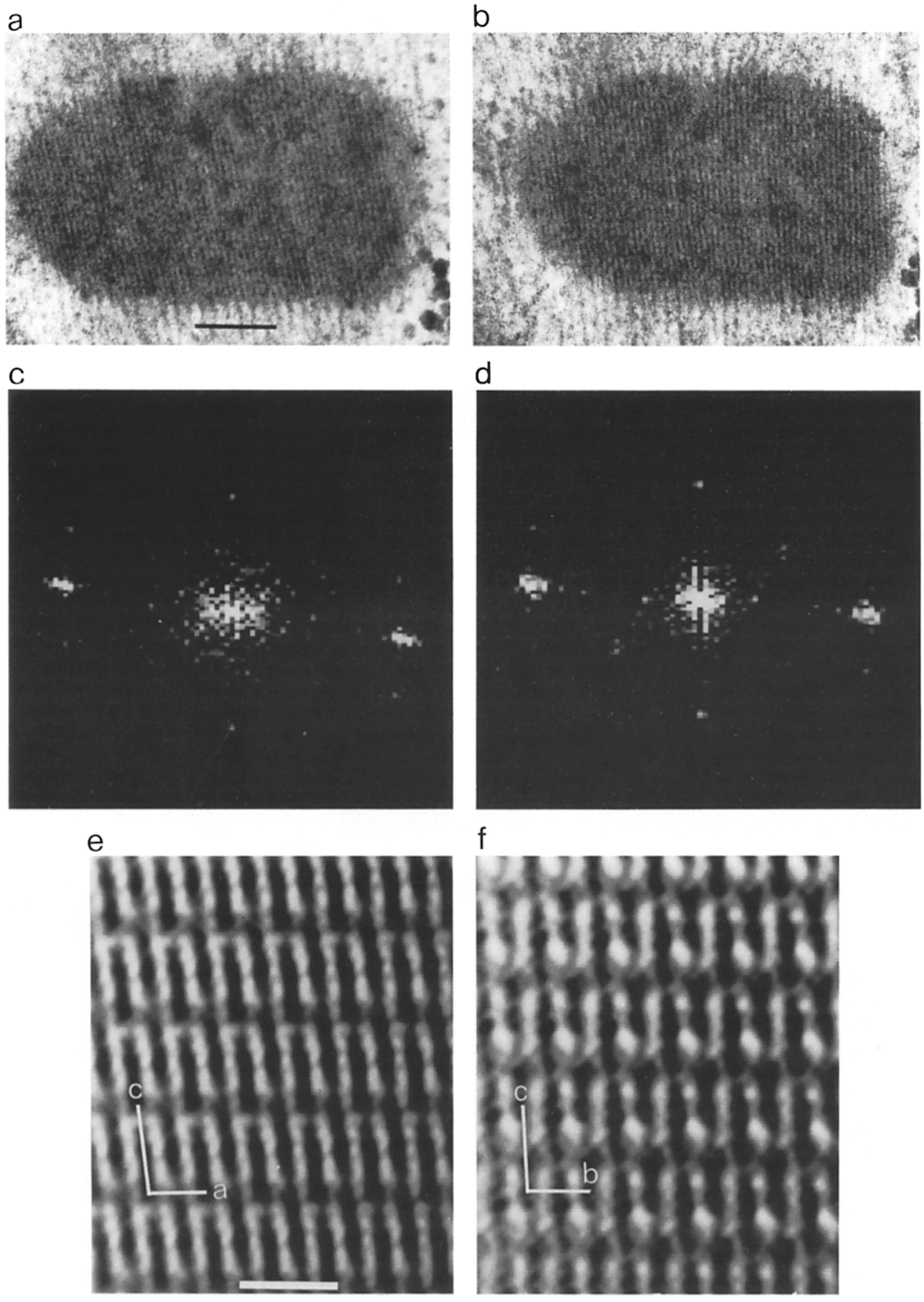
a
b
c
d
e
f
c
a
c
b

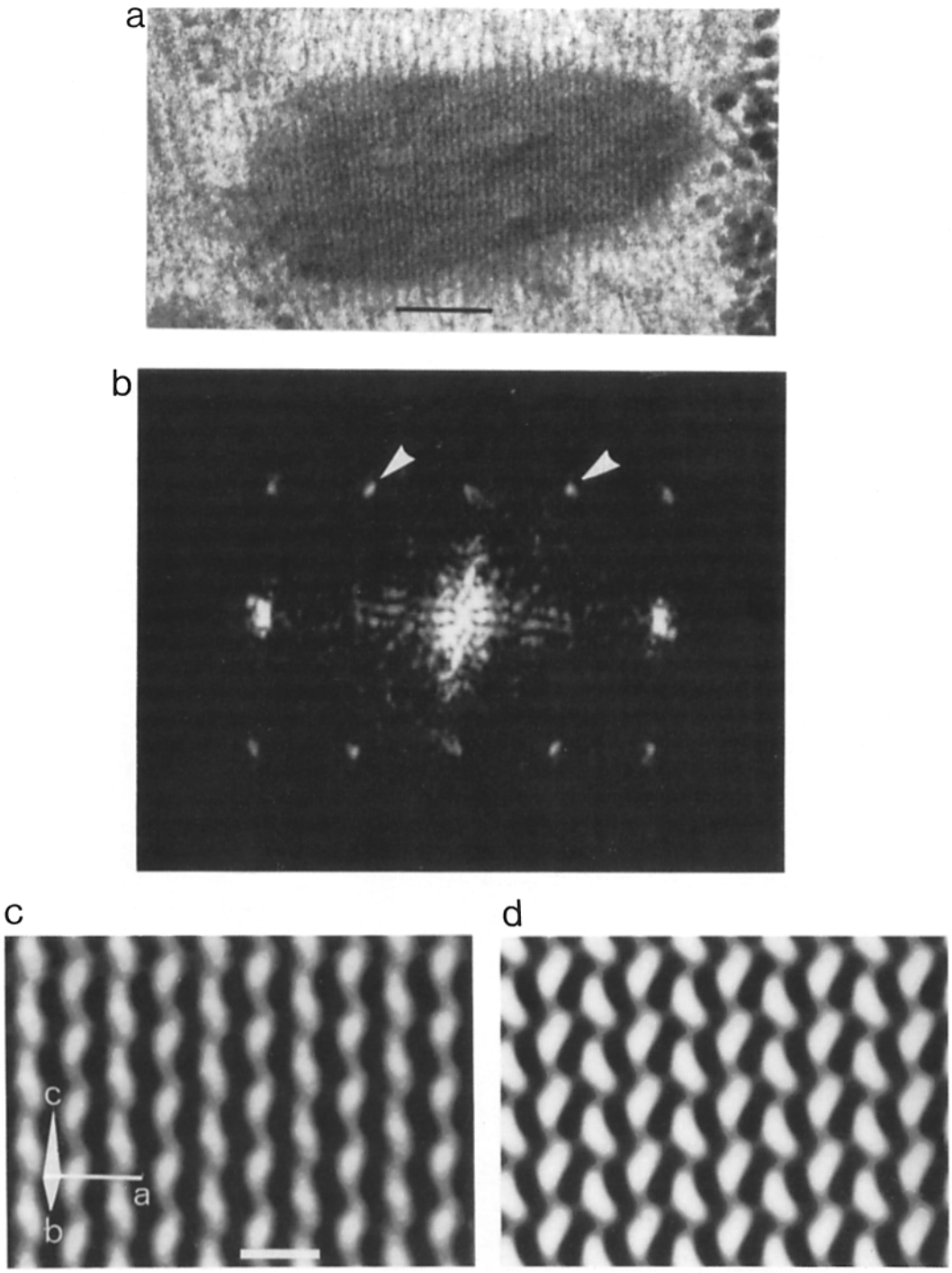


*Figure 8.* Tilted longitudinal view of nemaline Z-band. (*a*) Micrograph of a [1,0]-type longitudinal section that has been tilted by 60° about an axis normal to the filament axis (i.e., the *a* axis). (*b*) Computed diffraction pattern of *a*. The diffraction pattern samples the [−2,0,0] and [2,0,0] reflections on the equator and the [−2,1,1], [−1,1,1], [0,1,1], [1,1,1], and [2,1,1] reflections on the first layer-line. The [−1,1,1] and [1,1,1] reflections are marked with arrowheads. (*c*) Fourier-filtered image of *a*. The *a*, *b*, and *c* axes of the three-dimensional unit cell are marked. Dark areas represent protein. (*d*) Three-dimensional reconstruction of nemaline Z-band rotated and projected to match the orientation of *a* and *c*. Bars: (*a*) 200 nm; (*c* and *d*) 25 nm.

*Figure 7.* Longitudinal [1,0]- and [0,1]-type views of nemaline Z-band. (*a*) Micrograph of a [1,0] view corresponding to a [1,1]-type view tilted to 50° about a filament axis. (*b*) Micrograph of a [1,0] view corresponding to the same region as Fig. 7 *a*, this time tilted to −55° about a filament axis. (*c*) Computed diffraction pattern of *a*. (*d*) Computed diffraction pattern of *b*. (*e*) Fourier-filtered image of *a*. The *a* and *c* axes of the three-dimensional unit cell are marked. (*f*) Fourier-filtered image of *b*. The *b* and *c* axes of the three-dimensional unit cell are marked. Protein is dark. The tilt axis for the micrographs is parallel to the *c* axis. Note the similarity between *e* and *f*, except that the regions of lateral connection in *f* have been shifted by half a unit cell along the filament axes. Bars: (*a* and *b*) 200 nm; (*e* and *f*) 50 nm.

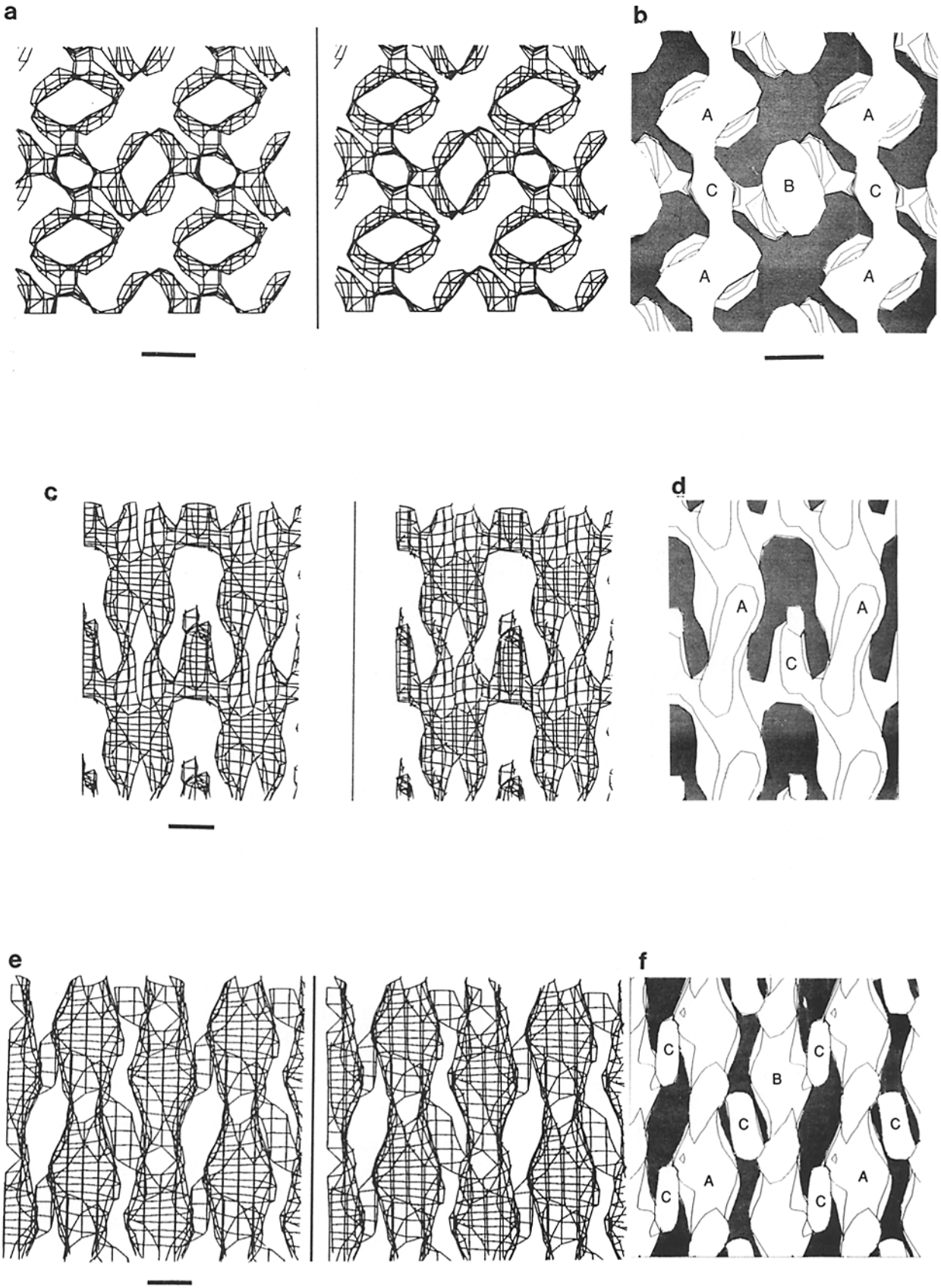


*Figure 9.* Views of the three-dimensional reconstruction of nemaline Z-band. Contoured surfaces are represented as chicken-wire in stereo using the program Frodo on the Evans and Sutherland PS300 graphics system (*a*, *c*, and *e*) and as stacked contours with hidden lines removed and a shaded background (*b*, *d*, and *f*). (*a* and *b*) Transverse views showing end on actin filaments which have a righthanded twist. Four filaments (labeled *A*) deriving from one side of the Z-band surround a fifth filament (labeled *B*) of the opposite polarity deriving

tween the zigzags. These results are exactly what is predicted from fourfold screw symmetry. However, they do depend on identifying common features between different tilted views. Since the shapes of the common features themselves tended to change between the different views this procedure was not always straightforward. Therefore we thought it desirable to check this observation by an independent method.

In the second method, a further tilt series of the longitudinal view was analyzed. In this case the section was tilted about an axis normal to the filament axes in the Z-band. The untilted view corresponded to a [1,0]-type view. From geometrical considerations tilting in this manner should produce a view in the computed diffraction pattern in which the [1,1,1] and [−1,1,1] reflections are sampled. Fig. 8, *a–c* shows a longitudinal view of a [1,0] projection tilted to 60° in this manner together with its computed diffraction pattern and filtered image. For fourfold symmetry the [1,1,1] and [−1,1,1] reflections (marked with arrows in Fig. 8 *b*) should have the same phase: for fourfold screw symmetry their phases should differ by 180°. This arises since these reflections are related by 90° rotation and therefore will have the same amplitude and phase in the case of fourfold rotational symmetry. In the case of fourfold screw symmetry, 90° rotation is combined with translation by one-fourth of the distance corresponding to a full 360° rotation of the helix. Since the first layer line in the transform corresponds to half a turn of the actin helix, these two reflections should have the same amplitude and should differ by 180° in phase. When the phase axis of the computed diffraction pattern in Fig. 8 *b* was adjusted to coincide with a filament axis, the phase shift being determined by examination of the [2,0,0] reflection, it was found that the phase difference between the [1,1,1] and [−1,1,1] reflections was 182°, thus strongly supporting the fourfold screw symmetry assignment. In addition the filtered image of this particular view (Fig. 8 *c*) is in close agreement with the equivalent projection of the reconstruction (Fig. 8 *d*) calculated using fourfold screw symmetry (see below).

### *Combining the Data in Three Dimensions*

Two separate three-dimensional reconstructions were calculated from the two tilt series obtained from longitudinal sections and tilted about an axis parallel to the filament axis. For each reconstruction the data were combined with the data from the transverse section shown in Fig. 2. The two reconstructions were very similar to each other: the reconstruction shown corresponds to the data in Figs. 2, 4, 5, and 6, in which reflections on the second layer line of the computed diffraction patterns were consistently stronger than in the other series. The observed fourfold screw symmetry was used to generate additional views since the rotation of the specimen holder was restricted to ± 60°. Without using this symmetry a total tilt of ± 90° would be required to collect all the data. To combine the data in reciprocal space, the reflections in the computed diffraction patterns were scaled and shifted to a common phase origin by comparing the amplitudes and phases of common reflections using an approach based on that described by Amos et al. (1982) for two-dimensional crystals. A phase origin located on an actin filament axis was chosen. Longitudinal views corresponding to a tilt series were approximately aligned in real space using common features and that was followed by more exact alignment using the reflections in the computed diffraction patterns. Longitudinal alignment in the direction of the *c* axis was made by reference to the [0,0,2] reflection, which was common to all longitudinal views. The phase difference between common reflections derived from different views was calculated by hand. A program was used to apply the appropriate phase shift to all reflections deriving from a particular view. Lateral alignment in the plane containing the *a* and *b* axes was made with reference to the transverse view in Fig. 2, which had previously been corrected so that the *a* and *b* axes were of equal length and the lattice angle was 90°. In the computed diffraction pattern of each longitudinal view, there is a single reflection that is also present in the computed diffraction pattern of the transverse view. In the case of the [1,0]-type view this is the [2,0,0] reflection; in the case of the [1,1]-type view this is the [1,1,0] reflection; and so on. The appropriate lateral phase shifts were calculated and applied as in the case of longitudinal alignment. The fourfold screw symmetry was also used to resolve the ambiguity in combining views related by 90° rotation caused by the absence of the first order reflection on the meridian. A further source of ambiguity arose in the case of the [2,1]- and [1,2]-type projections, in which the [2,1,0] and [1,2,0] type reflections are very weak in the computed diffraction pattern of the transverse view (Fig. 2 *b*) and so could not be used for origin refinement. In this case the mirror relationship between the [2,1,0] and [−2,−1,0] reflections arising from the fourfold screw symmetry was used starting out from the approximate alignment initially obtained in real space. This alignment could be tested by comparison with the computed diffraction pattern of the longitudinal section tilted about an axis perpendicular to the filament axis (Fig. 8 *b*) in which the [−2,1,1] and [2,1,1] reflections are also sampled. When these

from the other side of the Z-band. Linking structures (labeled *C*) to the left and to the right of the central filament (*B*) connect groups of four filaments (*A* and *B*). The region of reconstruction shown has been limited to about half a unit cell in the *c* direction: the complete unit cell would show the symmetry related linking structures above and below the central filament. (*c* and *d*) Longitudinal [1,0]-type side views of two filaments (labeled *A*) of the same polarity. The linking structure (labeled *C*) makes contacts with each filament at the same axial level and runs parallel to the filaments for ~18 nm towards the top of the page before forming links towards and away from the viewer. These connect to actin filaments of the opposite polarity located outside the region of reconstruction viewed here. The extent of the plot in the direction normal to the viewing plane has been limited for clarity. Regions of the filaments towards and away from the viewer have been sectioned away and are thus not enclosed by the contours. (*e* and *f*) Longitudinal [1,1]-type side views of three filaments (labeled *A* and *B*). The filament in the center (labeled *B*) is opposite in polarity to its two neighbors (labeled *A*). The polarity of the filaments can be identified by examination of the region where the linking structure (labeled *C*), Z-shaped in profile, joins the *B* filament and *A* filaments. The thickened region of the filament at this joint has a tadpole shape that points down for the center filament and up for the one on the left. The other set of linking structures between the center and righthand filaments is related to the first set by the fourfold screw and so the Z-profile is viewed edge on.

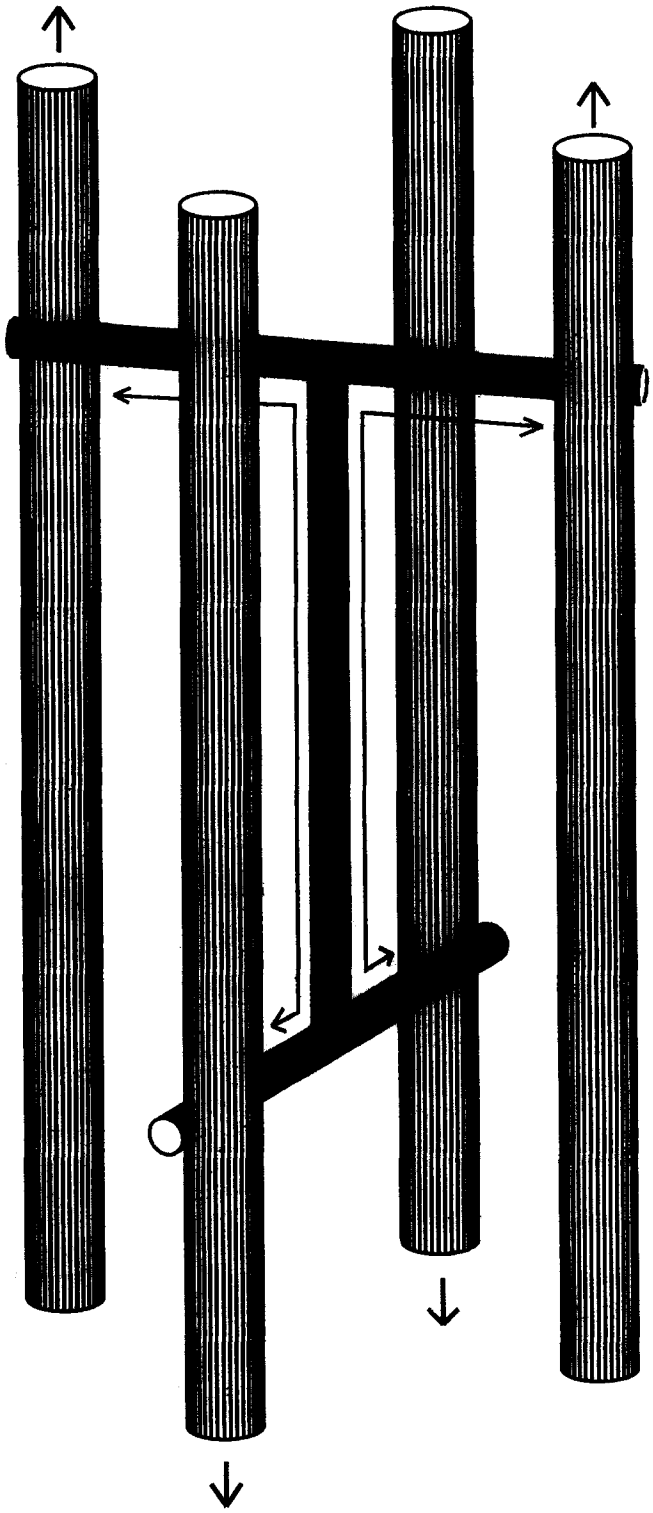

*Figure 10.* Schematic diagram of the linking structure (*black cylinders*), which makes contacts with four actin filaments (*lined cylinders*). The polarity of the actin filaments is identified by arrows, which point towards the edge of the Z-band from which the actin filament emerges: this also corresponds to the polarity of the chevrons formed by the links. It is suggested that each linking structure may be composed of two molecules of α-actinin as indicated by the two bent lines with arrowheads at each end.

were compared, the average phase error was 30° so this comparison supports the original assignment of the phase origin for the [2,1] projection based on the mirror relationship of the [2,1,0] and [−2,−1,0] reflections (see above). A similar procedure was used for the [1,2] projection.

In the process of merging different views of the nemaline Z-band it was necessary to correct for long-range distortions in the images. The most obvious and severe distortions seem to be (*a*) an apparent shearing of the lattice in the *x*–*y* plane, tentatively assigned to section compression, and (*b*) collapse in the z direction. The latter can be inferred from the angle needed to tilt from a [1,0]-type view to a [0,1]-type view, which was 105° in the case of Fig. 7. Assuming that the lattice was originally square, the angle should be 90°, and this would correspond to a shrinkage of ~23% compared with the *x*–*y* plane. This type of collapse has previously been observed and quantified in plastic sections (Bennett, 1974; Luther et al., 1988). To correct for these distortions, reflections with the same index in different views are treated as if they arose from an undistorted lattice. The underlying assumption is that the distortions involved are uniform so that distances and spacings are changed by a constant factor in any given direction. In their studies Bennett (1974) and Luther et al. (1988) concluded that section collapse occurred in this way.

The resolution of the reconstruction can be estimated from the highest order reflection included in the three-dimensional Fourier synthesis, in this case the [2,1,1] reflection, which corresponds to a spacing of 11.9 nm. From Fig. 6 *b* it can be seen that this reflection is well above the noise level, so it seems reasonable to interpret the reconstruction to this resolution with some confidence. It should also be emphasized that the resolution of the reconstruction is isotropic in the sense that there is no missing cone of data of the type frequently encountered in the analysis of two-dimensional crystals (Amos et al., 1982).

### *Three-dimensional Reconstruction*

The appearance of the three-dimensional reconstruction is illustrated in stereo contour chicken wire plots (Fig. 9, *a*, *c*, and *e*) and superimposed contours plots with hidden lines removed (Fig. 9, *b*, *d*, and *f*). Fig. 9, *a* and *b* are transverse views of the structure showing a central filament (labeled *B*) surrounded by four filaments (labeled *A*) which derive from the adjacent sarcomere. The filaments can be seen to have a righthanded twist characteristic of actin filaments. Linking structures (labeled *C*) are located to the left and right of the central filament. Closest to the viewer, links are formed between equivalent filaments (*A*) running up the page. The linking structures also run parallel to the filament axes away from the viewer to join up with another set of links running from left to right across the page which connect the central filament (*B*) to equivalent filaments to the left and right. The linking structures connect to the edge of the filaments at a tangent rather than pointing directly towards the filament axes. For the central filament (*B*) these connections have a clockwise sense. For the surrounding filaments (*A*) the sense is anticlockwise. Thus in transverse projection the linking structure resembles an X, whose arms cross at an angle of ~45° and run approximately parallel to [−2,1] and [−1,2] lattice vectors (this linking pattern in transverse view is also illustrated in Fig. 3).

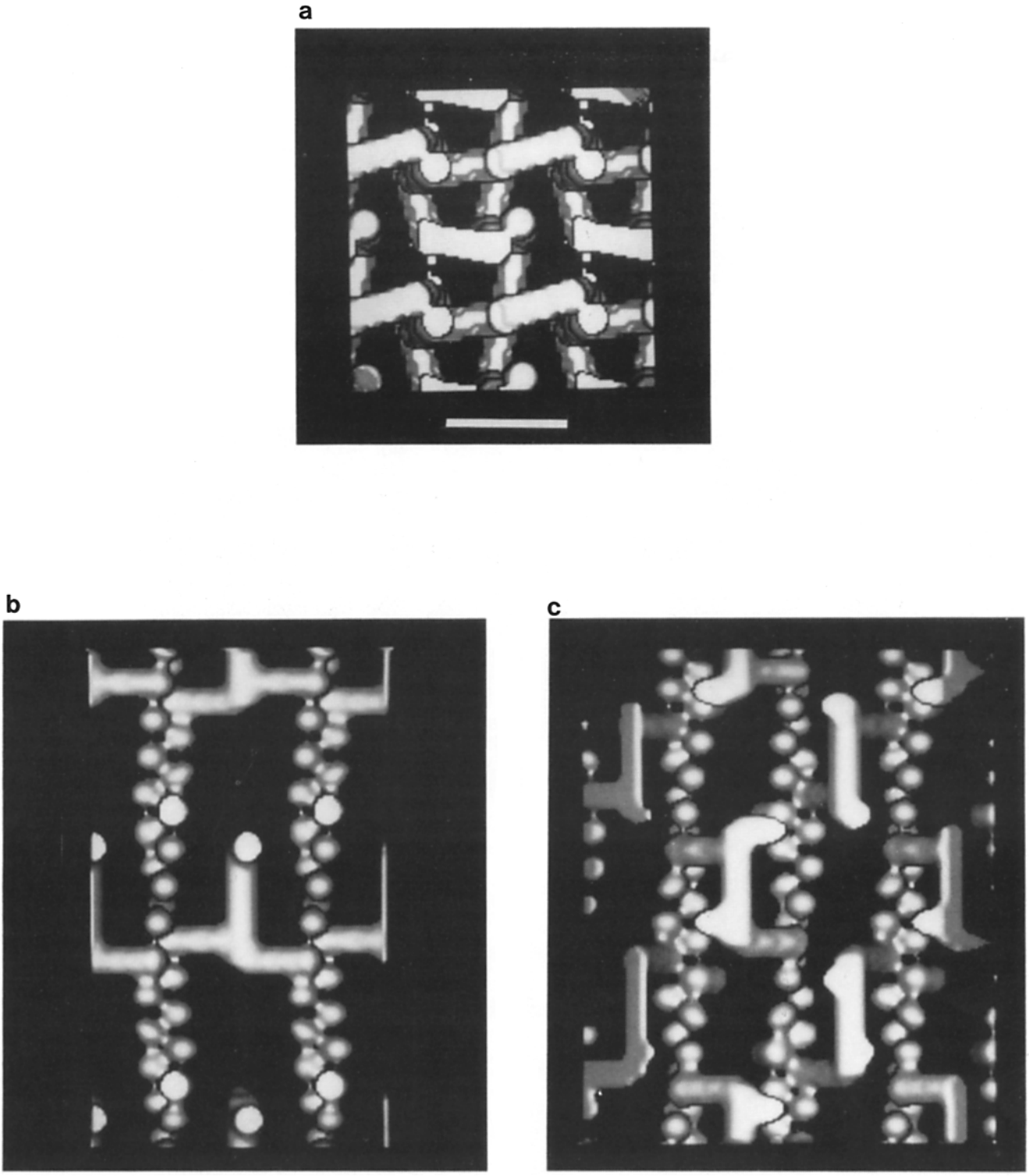


*Figure 11.* Models of the nemaline Z-band structure taking account of the subunit structure of actin. Three-dimensional density maps were constructed using spherical actin subunits (radius 2.4 nm) and helical actin filaments. The linking structures are composed of cylinders (radius 2.4 nm) incorporating the geometry of attachment observed in the three-dimensional reconstruction. Here the resulting map is illustrated in (*a*) transverse, (*b*) longitudinal [1,0], and (*c*) longitudinal [1,1]-type orientations using the surface representation program SURF written by G. Vigers (Medical Research Council Laboratory of Molecular Biology). These views can be compared with the equivalent views of the three-dimensional reconstruction in Fig. 10. Bar, 20 nm.

The axial extent of the linking structure can be more clearly seen in longitudinal plots of the reconstruction (Fig. 9, *c–f*). Fig. 9, *b* and *c* are plots of the [1,0] type longitudinal view showing two filaments (*A*) that derive from the same sarcomere. The plots have been restricted to contain a single layer of filaments. The righthanded twist of the filaments is again clearly shown. The segment of the linking structure (*C*) that runs parallel to the filaments is ~6 nm in diameter and its length corresponds to approximately a quarter turn of the filament helix. The appearance of the reconstruction

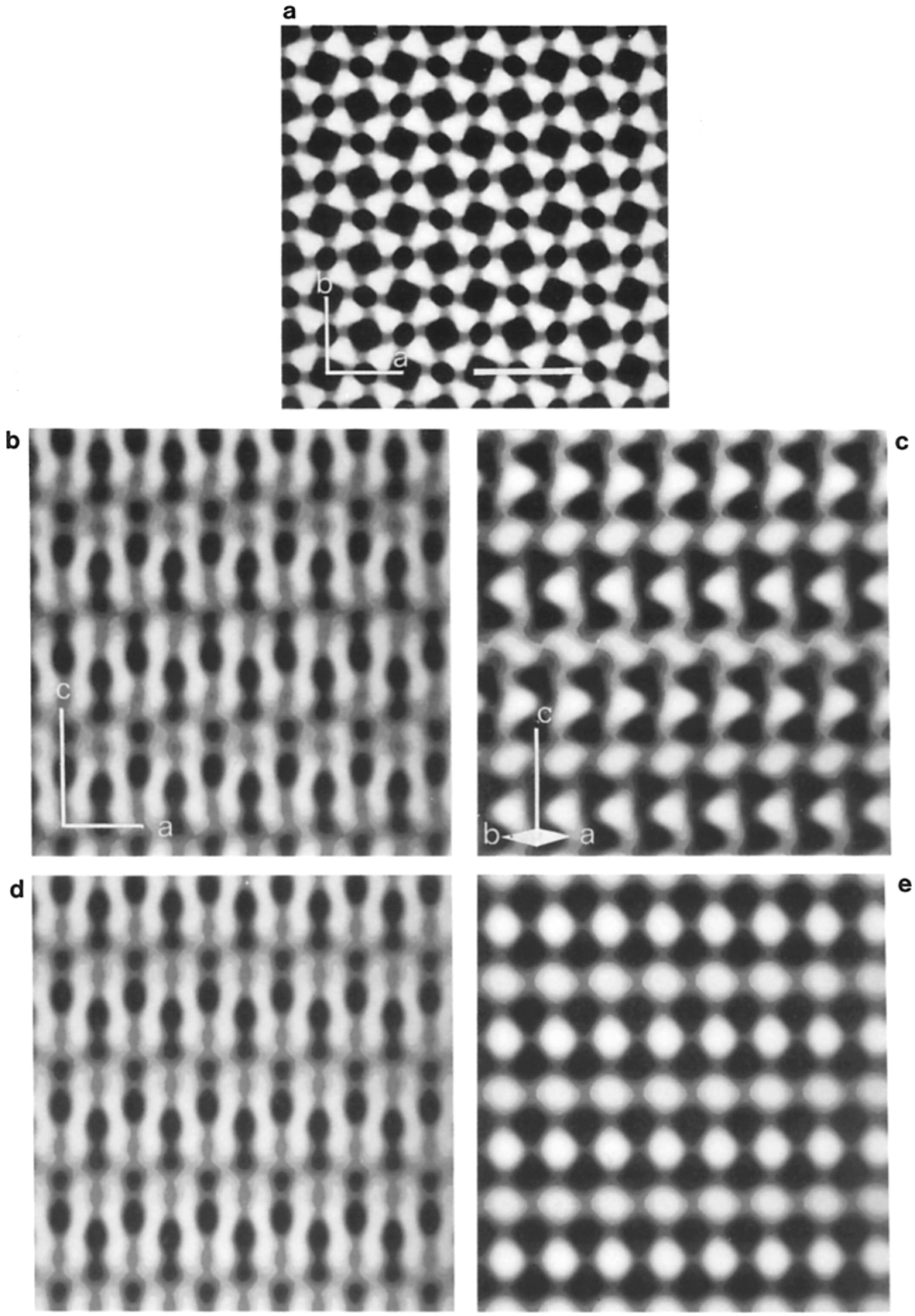


*Figure 12.* Two-dimensional projections of the model structure illustrated in Fig. 11. (*a*) Transverse; (*b* and *d*) longitudinal [1,0]; and (*c* and *e*) longitudinal [1,1]-type views. *b–e* have been Fourier filtered to approximate to the resolution obtained from electron micrographs of the nemaline Z-band. *d* and *e* have also been internally averaged by folding across the filament axes. These views can be compared with the Fourier-filtered images in Figs. 2 *c*, 4 *c*, and 5 *c*, respectively. Bar, 40 nm.

can be related to the two-dimensional Fourier synthesis of the [1,0] view (Fig. 4 *c*). The arms of the linking structure connecting to the filaments in the reconstruction contribute to the zigzags linking the filaments in the Fourier synthesis. The region of the linking structure running parallel to the filaments reinforces the filament density on one side of the zigzag, thus emphasizing the reverse polarity of adjacent filament projections in the Fourier-filtered image.

Longitudinal views of the two classes of filaments (*A* and *B*) are seen in the plots of the [1,1]-type longitudinal view in which a single layer of filaments is included (Fig. 9, *e* and *f*). The opposite polarity of the A and B type filaments is indicated by the tadpole-shaped bulges formed where the linking structures (*C*) join the filaments. The linking structure on the left side of the central filament (*B*) presents a Z-shaped profile to the viewer, while in the case of the linking structures on the righthand side the Z is viewed edge on. As a consequence of the fourfold screw symmetry, the views of the linking structures at different axial levels are related by 90° rotation. The difference in appearance between these views arises from the orientation of the arms of the linking structure which connect to the central filament with a clockwise sense and to the adjacent filaments with an anticlockwise sense as noted for the transverse view.

From these views of the reconstruction, it can be seen that the linking structure is located in a central position between four filaments (Fig. 10) and serves to connect two pairs of filaments of opposite polarity.

### *Modeling of the Three-dimensional Reconstruction*

Due to the limited resolution of the reconstruction, the actin filaments appear as continuous two-stranded helices without any subunit detail. Since it is likely that the linking structures are attached at each end specifically to one or more actin subunit in the structure, we constructed a three-dimensional model of the Z-crystal, in which the actin filaments are composed of spherical subunits and the ends of the linking structures are attached to single actin subunits with the geometry observed in the reconstruction. This is illustrated in surface representations of the transverse and longitudinal [1,0] and [1,1] views in Fig. 11 (*a–c*) corresponding to the contour maps of the reconstruction in Fig. 9. Helical symmetry of 28 subunits in 13 turns was used for the actin so that the observed fourfold screw symmetry in the reconstruction was incorporated into the actin filaments themselves. In this way, equivalent interactions could be made for each contact between actin subunits and linking material. The resulting model has lefthanded screw symmetry. Comparison shows quite good correspondence between the model and the reconstruction. Projections of the model along the filament axes and in [1,0] and [1,1] longitudinal directions Fourier filtered to approximately the same resolution as the original data are shown in Fig. 12. These can be compared with the Fourier-filtered images from the original micrographs (Figs. 2 *c*, 4 *c*, and 5 *c*). Again they show quite good agreement; in particular the zigzags running across the crystal are well reproduced in Fig. 12, *b* and *d*.

## *Discussion*

### *Symmetry of the Z-Crystal*

For the purpose of calculating the reconstruction, only fourfold screw symmetry was used. However, it is apparent both from the reconstruction and from the filtered images of the micrographs used in the reconstruction that there is additional symmetry present that relates the filaments which derive from the different sarcomeres. The [1,0] and [0,1] longitudinal projections have the appearance of pgg and pmg symmetry, indicating that the two types of filament are related by $2_1$ screw symmetry axes running parallel to the *a* and *b* axes. Examination of the reconstruction in longitudinal [1,1] view, and also the observation that the [1,2] and [2,1] projections are related by a reversal in polarity suggest that there are also twofold rotation axes running along the diagonal of the *a* and *b* axes passing through the centers of the linking structures, again relating the two types of filament. Taking into account these observations, the overall symmetry of the reconstruction is probably $P4_22_12$ with the fourfold screw axis along the actin filaments.

### *Relating the Z-Crystal Symmetry to That of the Actin Filaments*

At this stage, it should be noted that the observed $P4_2$ symmetry implies twofold rotational symmetry along the actin filament axes. From the known subunit structure of the actin filament, exact twofold symmetry is not possible since actin subunits on opposite long pitch strands are related by translation of 2.75 nm and rotation by ~167°. The precise helical symmetry and long-pitch periodicity of actin filaments can vary in different systems, for example, in insect flight muscle the symmetry is 28/13 (28 subunits in 13 turns of the genetic helix) with a long-pitch periodicity of 76.8 nm (Miller and Tregear, 1972), whereas in vertebrate skeletal muscle the long pitch periodicity is in the range 72–74 nm, corresponding to a helical symmetry of between 28/13 and 13/6 (Huxley and Brown, 1967). In addition, there is evidence that actin filaments can be rotationally flexible, as shown by the cumulative angular disorder observed in isolated actin filaments by Egelman et al. (1982). Although it is not possible for the actin filaments to have $4_2$ screw symmetry, it is possible for them to possess $4_3$ symmetry if they adopt 28/13 symmetry.

Bearing these constraints in mind, we have considered two types of interpretation of the reconstruction: (*a*) that the screw symmetry of the structure is $4_3$, incorporating 28/13 helical symmetry in the actin. In this case, all the links between the filaments are equivalent, as seen in Figs. 11 and 12, and the true symmetry of the model is $P4_32_12$. Although not possessing $4_2$ symmetry, the structure may have that appearance at low resolution. (*b*) The actin helical symmetry does not incorporate a fourfold screw axis. In this case, the actin helix and/or the links might be distorted to optimize the bonding. The apparent twofold rotational symmetry might then arise from the averaging of filaments with different bonding patterns. In both cases, the twofold rotational symmetry in the projected images could also be due to a type of disorder in which the filaments with the same polarity but rotated by 180° about their axes with respect to each other are averaged together, as is suggested to occur in insect flight muscle (Miller and Tregear, 1972). The feasibility of the first interpretation is addressed in our modeling studies. The [1,0] projection derived from this model (Fig. 12 *b*) comes quite close to the appearance of twofold rotational symmetry about the filament axes. The [1,1] projection

(Fig. 12 *c*) is less satisfactory in this respect; here the symmetry along the filament axes is clearly $2_1$. Other models in which the axial component of the linking structure is longer come much closer to having a twofold axis at this resolution; however, their overall appearance matches the experimental [1,1] views less well. Alternatively, closer agreement with the observed [1,1] (and also [1,0]) views is obtained if filaments are averaged by rotation about their axes by 180°, thus converting the $2_1$ screw axes into twofold rotation. This is illustrated for both the [1,0] and [1,1] views in Fig. 12, *d* and *e*.

### *Comparison with Previous Electron Microscope Images of the Z-Band*

Two appearances have been described for transverse sections of vertebrate skeletal and cardiac muscle Z-bands, which are commonly referred to as the basketweave and small-square lattices (Reedy, 1964; Landon, 1970). The basketweave lattice appears to possess curved connections running approximately diagonally between nearest neighbor filaments. In the small-square lattice, connections between filaments appear to run directly between filaments of the same polarity with apparent overlap in the central region. Transverse sections of the nemaline rod Z-crystal correspond to the small square lattice: the appearance is very similar to that described for this type of lattice in canine cardiac muscle (Goldstein et al., 1979) and rat soleus muscle (Goldstein et al., 1987). In transverse projection, the structure has fourfold rotational symmetry as pointed out in their earlier work. However, our analysis from tilted longitudinal sections shows that, at least in the case of the nemaline Z-band, this arises from fourfold screw symmetry. This type of symmetry, unlike fourfold rotational symmetry, allows links to the actin filaments to be equivalent or nearly equivalent depending upon the exact helical symmetry of the actin.

Longitudinal [1,0] images show some resemblance to the optical reconstructions of extracted nemaline Z-bands (Goldstein et al., 1980), although the optical diffraction patterns in these studies show strong first-order reflections on the equator and meridian, in contrast to the present study, in which these reflections were either very weak or absent. It is possible that the extraction procedure is responsible for this difference. The longitudinal [1,0] images have a zigzag appearance generally characteristic of the Z-band. In particular, the averaged longitudinal images of plantaris Z-bands with three or four levels of chevrons obtained by Rowe (1973) are quite similar to our longitudinal [1,0] images.

### *Relationship of the Reconstruction to Previous Studies of the Z-Band*

Quite a variety of three-dimensional models have been proposed for the Z-band based on electron microscope studies. Most have derived from interpretations of electron micrographs of thin sections of particular views of the structure. Since even the thinnest section (for example, 20 nm) is likely to include several levels of the structure that are superimposed and imaged as a projection in the electron microscope, it is not surprising to find a diversity of models that are apparently consistent with the data available from a single view. Three-dimensional reconstruction from tilted sections provides a more objective means of obtaining the Z-band structure.

Recently, two three-dimensional analyses of different Z-bands have been obtained. Cheng and Deatherage (1989) and Deatherage et al. (1989) have calculated three-dimensional reconstructions of the honeybee flight muscle Z-band. In this type of muscle the actin filaments are arranged in a hexagonal lattice in contrast to the square lattice characteristic of vertebrate skeletal and cardiac muscle. Their reconstruction shows the regions of overlap and termination of the filaments together with linking elements. The unit cell in this type of Z-band is rather larger and more complicated than the nemaline Z-crystal. There are, however, a number of consistent features in the linking structures of the two reconstructions. Both maps show a region where the linking structures run parallel to the actin filaments for ~20 nm and make contact with filaments from adjacent sarcomeres.

A second, more closely related reconstruction has been obtained from the Z-band of fish white muscle (Luther, P. K., manuscript submitted for publication). In this case, transverse sections have an appearance intermediate between the small-square and basketweave lattices. Connections run between actin filaments of opposite polarity deriving from adjacent sarcomeres and show a region running parallel to the filament axes. On each side of the Z-band, there appear to be links in one direction between filaments from the same sarcomere. A possible interpretation of these links is that they correspond to the region in the nemaline Z-crystal reconstruction where the linking structure connects filaments of the same polarity. As with the nemaline Z-crystal, links in the fish reconstruction are made to the four surrounding actin filaments deriving from the adjacent sarcomere. It is clear that these links at 90° are not at the same axial level. It is not clear as yet whether their axial displacement corresponds to a quarter turn of the actin helix as observed in the nemaline Z-crystal.

One common feature of these reconstructions is that the actin filaments run continuously through and terminate in the Z-band as proposed in the model of Knappeis and Carlsen (1962), in contrast to the looping arrangements suggested in some models (Rowe, 1973; Ulrick et al., 1977). By comparing the longitudinal views with the final reconstruction of the nemaline Z-band it can be seen that much of the contrast in the longitudinal views derives from the linking structures rather than the actin filaments. Without the three-dimensional density map, this might well give the impression that actin filaments follow paths that we would interpret as corresponding to the linking structures.

### *Interpretation of the Nemaline Z-Crystal Reconstruction*

The work of Yamaguchi et al. (1978) shows that the filaments running through the nemaline Z-crystals are composed of actin. In our reconstruction the filaments running through the structure appear as ribbons with a righthanded twist. It therefore seems reasonable to ascribe this twist to the actin long-pitch helix. The width of the filaments (~17 nm) is rather greater in the region of attachments of links to the filaments than in the region between attachment sites (~15 nm). Since the maximum diameter of the actin filaments is generally considered to be in the range of 9–10 nm (O'Brien et al., 1983; Egelman and Padron, 1984) part of the filament should be interpreted as linking material in the region of link attachment and possibly in the regions between.

Yamaguchi et al. (1978) have also demonstrated that the structure contains α-actinin and that its extraction leads to the loss of transverse striations in the Z-crystal. Since the bridging regions of the linking structures in the reconstruction are responsible for these transverse striations, it seems reasonable to suggest that the linking structure is part or wholly composed of α-actinin. The linking structure makes four contacts with actin filaments: α-actinin is a rod-shaped dimer ~40 nm long and ~4.5 nm in diameter (Polubnaya et al., 1975; Suzuki et al., 1976) and is probably composed of two antiparallel monomers (Walraff et al., 1986). Therefore it seems likely that each linking structure is composed of two α-actinin dimers running between actin filaments of opposite polarity deriving from adjacent sarcomeres, as illustrated in Fig. 10. The path length ascribed to α-actinin would be ~36 nm, which agrees quite well with measurements of its molecular length noted above.

According to this interpretation of the linking structure, the region in which it forms a strand running parallel to and between the actin filaments is composed of two α-actinin dimers. The present limited resolution of our reconstruction makes it difficult to decide whether the α-actinin dimers are making contact over part or all of this region or simply running close together. An interaction between α-actinin dimers would be of some general interest: present knowledge of α-actinin suggests that it is a divalent cross-linker of actin filaments. If the cross-linking molecules themselves can be cross-linked, a higher degree of complexity can be introduced into the system.

### *Geometry of the Interaction between α-Actinin and Actin*

The linking structures interpreted as α-actinin connect to the edge of the actin filaments at a tangent (Fig. 9, *a* and *b*). This suggests that contact is made primarily to one strand of the actin long-pitch helix as, for example, in myosin head binding. The opposite sense of the interaction associated with filaments from adjacent sarcomeres shows that a single type of site on the actin is involved. This part of the map bears some resemblance to reconstructions of actin decorated with S1 (Milligan and Flicker, 1987; Vibert and Craig, 1982; Toyoshima and Wakabayashi, 1985). The limited resolution of our reconstruction means that it is not possible to determine the axial extent of the interaction: the simplest arrangement would be for a single actin subunit to be involved, as illustrated in our models of the structure (Fig. 11), but it is possible that the interaction is spread over as many as three subunits on the same long-pitch strand. It has been observed that α-actinin competes with tropomyosin in its binding to actin filaments (Goll et al., 1972; Stromer and Goll, 1972). Tropomyosin is thought to be located at a radius of ~4 nm from the actin filament axis (O'Brien et al., 1983; Milligan and Flicker, 1987). If the competition is due to a direct effect this would place the binding site for α-actinin at a similar radius, which would be consistent with our reconstruction in which the α-actinin appears to join the edge of the actin filament at high radius.

### *The Relationship of the Nemaline Z-Band to Small-Square and Basketweave Z-Bands*

As discussed above, Z-bands have frequently been classified on the basis of their transverse appearance into basketweave and small-square appearance. The nemaline Z-band appears to belong to the small-square class. It is probably the case that the three-dimensional structure we have described for the nemaline Z-band can be applied to other small-square Z-bands. However, it is important to note that the part of the structure analyzed here is limited to the repeating region in the center of the structure. There may well be significant differences between this region and the edges of the Z-band where the actin filaments terminate. A characteristic feature of the small-square lattice is that in transverse view, the linking structures appear to run between actin filaments of the same polarity. This feature appears in the nemaline Z-band reconstruction where, for example, in Fig. 9 *a* links running up the page join the A-type filaments and links running from left to right across the page join the B-type filaments. The reconstruction shows that these two sets of links occur at different axial levels and are joined together by the central part of the linking structure which runs axially. The basketweave lattice, conversely, appears to be characterized by links running between actin filaments of opposite polarity. However, our interpretation of the linking structure, namely that it is composed of two α-actinin dimers that are connected at each end to actin filaments of opposite polarity (Fig. 10), appears to be consistent with the apparent connectivity in the basketweave lattice. Therefore it might be possible to generate the basketweave appearance if the two α-actinin dimers were to separate or move further apart in the region where they run together axially. This suggestion corresponds quite closely with the model for small-square to basketweave transition proposed by Goldstein et al. (1986). The most satisfactory way of addressing this question is by comparison with a three-dimensional reconstruction of a basket-weave type Z-band. Lee (1989) has carried out several such reconstructions from the frog skeletal muscle Z-band: however, at the present stage of the analysis the maps are too noisy to make a clear interpretation of the linking elements in the structure. We hope to extend this work.

We would like to thank Dr. M. Cullen (Newcastle General Hospital) for supplying the blocks of nemaline myopathy specimens, Dr. Pradeep Luther (Imperial College, London) for help and advice during the course of the project, and Dr. Pauline Bennett (Kings College, London) for critical reading of the manuscript.

This work was supported by a British Heart Foundation project grant. We acknowledge grants from the Wellcome Foundation and the Medical Research Council for the electron microscope and computer equipment.

Received for publication 23 May 1990 and in revised form 11 September 1990.

#### *References*

Amos, L. A., R. Henderson, and P. N. T. Unwin. 1982. Three-dimensional structure determination by electron microscopy of two-dimensional crystals. *Prog. Biophys. Mol. Biol.* 39:183–231.

Bennett, P. M. 1974. Decrease in section thickness on exposure to the electron beam; the use of tilted sections in estimating the amount of shrinkage. *J. Cell Sci.* 15:693–701.

Cheng, N., and J. F. Deatherage. 1989. Three-dimensional reconstruction of the Z disk of sectioned bee flight muscle. *J. Cell Biol.* 108:1761–1774.

Deatherage, J. F., N. Cheng, and B. Bullard. 1989. Arrangements of filaments and cross-links in the bee flight muscle Z disk by image analysis of oblique thin sections. *J. Cell Biol.* 1775–1782.

Egelman, E. H., and R. Padron. 1984. X-ray diffraction evidence that actin is a 100 Å filament. *Nature (Lond.)* 298:131–135.

Egelman, E. H., N. Francis, and D. J. DeRosier. 1982. F-actin is a helix with a random variable twist. *Nature (Lond.).* 298:131–135.

Goldstein, M. A., J. P. Schroeter, and R. L. Sass. 1979. The Z lattice in canine cardiac muscle. *J. Cell Biol.* 83:187–204.

Goldstein, M. A., M. H. Stromer, J. P. Schroeter, and R. L. Sass. 1980. Optical reconstruction of nemaline rods. *Exp. Neurology.* 70:83–97.

Goldstein, M. A., L. H. Michael, J. P. Schroeter, and R. L. Sass. 1986. The Z-band lattice in skeletal muscle before, during and after tetanic contraction. *J. Muscle Res. Cell Motil.* 7:527–536.

Goldstein, M. A., L. H. Michael, J. P. Schroeter, and R. L. Sass. 1987. Z band dynamics as a function of sarcomere length and the contractile state of muscle. *FASEB J.* 1:133–142.

Goll, D. E., A. Suzuki, J. Temple, and G. R. Holmes. 1972. Studies on purified α-actinin. I. Effect of temperature and tropomyosin on the α-actinin/F-actin interaction. *J. Mol. Biol.* 67:469–488.

Huxley, H. E., and W. Brown. 1967. The low-angle X-ray diagram of vertebrate striated muscle and its behaviour during contraction and rigor. *J. Mol. Biol.* 30:383–434.

Knappeis, C. G., and F. Carlsen. 1962. The ultrastructure of the Z-disc in skeletal muscle. *J. Cell Biol.* 13:323–335.

Landon, D. N. 1970. The influence of fixation upon the fine structure of the Z-disc of rat striated muscle. *J. Cell Sci.* 6:257–276.

Lee, J. 1989. Three-dimensional reconstruction of the vertebrate muscle Z-band. Ph.D. thesis, London University, London, England.

Luther, P. K., M. C. Lawrence, and R. A. Crowther, 1988. A method for monitoring the collapse of plastic sections as a function of electron dose. *Ultramicroscopy.* 24:7–18.

Miller, A., and R. T. Tregear. 1972. Structure of insect flight muscle in the presence and absence of ATP. *J. Mol. Biol.* 70:85–104.

Milligan, R. A., and P. F. Flicker. 1987. Structural relationships of actin, myosin, and tropomyosin revealed by cryoelectron microscopy. *J. Cell Biol.* 105:29–39.

Misell, D. L. 1978. Image analysis and interpretation. *In* Practical Methods in Electron Microscopy. 7th ed. A. M. Glauert, editor. Elsevier North-Holland Publishing Company, Amsterdam. 125–197.

O'Brien, E. J., J. Couch, G. R. P. Johnson, and E. P. Morris. 1983. Structure of actin and the thin filament. *In* Actin: Structure and Function in Muscle and Non-muscle Cells. C. dos Remedios and J. Barden, editors. Academic Press, Sydney, Australia. 1–15.

Polubnaya, Z. A., L. A. Tskhovrebova, M. M. Zaalishvili, and G. A. Stefanenko. 1975. Electron microscopic study of α-actinin. *J. Mol. Biol.* 92:357–359.

Reedy, M. K. 1964. Electron microscopic examination of the structure of the Z-band. *Proc. R. Soc. Lond. B. Biol. Sci.* 160:458–460.

Rowe, R. W. D. 1973. The ultrastructure of the Z discs from white, intermediate, and red fibres of mammalian striated muscles. *J. Cell Biol.* 57:261–277.

Squire, J. M. 1981. The structural basis of muscle contraction. Plenum Publishing Corp., New York/London.

Stromer, M. H., and D. E. Goll. 1972. Studies on purified α-actinin: II electron microscopic studies on the competitive binding of α-actinin and tropomyosin to the Z-line extracted muscle. *J. Mol. Biol.* 67:489–494.

Suzuki, A., D. E. Goll, I. Singh, R. E. Allen, R. M. Robson, and M. H. Stromer. 1976. Some properties of purified skeletal muscle α-actinin. *J. Biol. Chem.* 251:6860–6870.

Toyoshima, C., and T. Wakabayashi. 1985. Three-dimensional image analysis of the complex of thin filaments and myosin molecules from skeletal muscle. IV. Reconstruction from minimal- and high-dose images of the actin-tropomyosin-myosin subfragment-1 complex. *J. Biochem. (Tokyo).* 97:219–243.

Ullrick, W. C., P. A. Tosselli, J. D. Saide, and W. P. C. Phear. 1977. Fine structure of vertebrate Z-discs. *J. Mol. Biol.* 115:61-74.

Vibert, P., and R. Craig. 1982. Three-dimensional reconstruction of thin filaments decorated with $Ca^{2+}$-regulated myosin. *J. Mol. Biol.* 157:299–319.

Walraff, E., M. Schleicher, M. Moderstitzki, D. Reiger, G. Isenberg, and G. Gerisch. 1986. Selection of Dictyostelium mutants defective in cytoskeletal proteins: use of an antibody which binds to the ends of α-actinin rods. *EMBO (Eur. Mol. Biol. Organ.) J.* 5:61–67.

Yamaguchi, M., R. M. Robson, M. H. Stromer, D. S. Dahl, and T. Oka. 1978. Actin filaments form the backbone of nemaline myopathy rods. *Nature (Lond.).* 271:265–267.